Journal of Solid State Chemistry **166,** 58–66 (2002)
doi:10.1006/jssc.2002.9559, available online at http://www.idealibrary.com on IDEAL®

Synthesis, Electrical Properties, and Powder Neutron Crystal Structure Refinement of $Pb_{1-x}Bi_xPt_2O_4$ Compounds ($0 \leq x \leq 0.3$)

S. Obbade,*,[1] N. Tancret,* F. Abraham,* and E. Suard†

*Laboratoire de Cristallochimie et Physicochimie du Solide UPRESA 8012 CNRS, ENSCL- USTL, BP 108, 59652 Villeneuve d'Ascq, Cedex, France; and †ILL, avenue des Martyrs, BP 156, 38042 Grenoble, Cedex 9, France

Received November 1, 2001; in revised form February 11, 2002; accepted February 22, 2002

Substitution of Pb for Bi in the recently characterized mixed-valence lead–platinum oxide $PbPt_2O_4$ was attempted and a $Pb_{1-x}Bi_xPt_2O_4$ solid solution was obtained for $0 \leq x \leq 0.3$. Powder X-ray diffraction study showed that all substituted compounds crystallize with similar triclinic unit cell and $PbPt_2O_4$ lattice parameters. The structural model of $Pb_{0.7}Bi_{0.3}Pt_2O_4$ was refined from powder X-ray diffraction data using the Rietveld method and the results indicate the same crystal structure than $PbPt_2O_4$ with one mixed Pb/Bi atomic site. Neutron diffraction realized on the two limit compositions of the solid solution ($x = 0$ and 0.3) allowed to confirm the $PbPt_2O_4$ and $Pb_{0.7}Bi_{0.3}Pt_2O_4$ stoichiometries. Mean oxidation degree of Pt atoms in the $[PtO_4]$ infinite chains decreases from + 3 for $PbPt_2O_4$ to + 2.7 for $Pb_{0.7}Bi_{0.3}Pt_2O_4$. Conductivity measurements show a metallic behavior for all the compositions except the limit composition $x = 0.3$ for which a semiconducting behavior appears. © 2002 Elsevier Science (USA)

Key Words: **mixed valences oxide; electrical transition; powder neutron diffraction; Rietveld refinement.**

INTRODUCTION

Binary and ternary platinum oxides have been extensively studied for their electrical properties and the potential use of their electrochemical and catalytic properties. In oxides, platinum cations present two types of environment depending on their valence state: tetravalent platinum adopts octahedral coordination PtO_6, divalent or partially oxidized platinum is in square planar coordination PtO_4. The structure and properties of binary and ternary platinum oxides have been reviewed by Schwartz and Prewitt (1).

In our laboratory, the studies are focused on oxides based on Bi^{3+} or Pb^{2+}, two lone pair containing cations. Thus, the studied platinum oxides pertain to the Bi–Pb–Pt–O system.

In the Pb–Pt–O system two phases were reported: Pb_2PtO_4 (2) and $PbPt_2O_4$ (3). The first one contains Pt^{4+} in octahedral coordination, the PtO_6 octahedra are edge shared to form rutile-type chains. The chains are connected by Pb^{2+} ions. This compound is an insulator. The structure of the latter has been solved from X-ray powder diffraction data. It consists of PtO_6 octahedra (Pt^{4+}) and two types of PtO_4 square planes containing divalent and/or partially oxidized platinum.

In the Bi–Pt–O system, two compounds have been obtained for Bi/Pt = 1 at 700°C under 3 kbar of pressure (4). The pyrochlore-type $Bi_2Pt_2O_7$ is prepared as a single phase and exhibits a semiconducting behavior. The second compound with approximate composition $BiPtO_{3.5}$ adopts a $KSbO_3$-type structure and its structure is very much like that found for $Bi_3Ru_3O_{11}$ (5), and its ideal composition may be $Bi_3Pt_3O_{11}$. The two cubic structures are based on octahedral frameworks. The PtO_6 octahedra are linked by corners only in the pyrochlore structure and by edges and corners in the $KSbO_3$-type structure.

Finally, in the Bi–Pb–Pt–O system a series $Bi_{2-x}Pb_xPtO_4$ has been stabilized within the range $0.33 \leq x \leq 0.52$ (6). The structure consists of PtO_4 groups which are stacked along the *c*-axis of the tetragonal cell, and the (PtO_4) columns are linked together by Bi^{3+} and Pb^{2+} ions (7). Isostructural Bi_2MO_4 compounds exist for $M^{2+} = Cu^{2+}$ and $M^{2+} = Pd^{2+}$ (8, 9), on the contrary Bi_2PtO_4 has not been isolated, the stabilization of the compound is achieved by oxidation of platinum resulting from the substitution of Pb^{2+} for Bi^{3+}. Bi_2CuO_4 is an insulator, Bi_2PdO_4 is a semiconductor, oxidized lead–bismuth platinum phases exhibit semiconducting behavior with relatively high conductivity with small variations of conductivity values with the mean oxidation degree of the platinum atom (10). The structural features of the Bi or Pb platinum oxides have been confirmed by a photoelectron spectroscopy study (11). As in the $Bi_{2-x}Pb_xPtO_4$ series, variation of oxidation degrees of platinum atoms in $PbPt_2O_4$ can also be expected by substitution of Bi^{3+} for Pb^{2+}.

[1] To whom the correspondence should be addressed. Fax: + 33-320436814. E-mail: obbade@ensc-lille.fr.

0022-4596/02 $35.00

The aim of this paper is to study the effect of Bi^{3+} for Pb^{2+} substitution in $PbPt_2O_4$ on the structure, eventually on the oxygen non-stoichiometry and on the conductivity properties. We report here the synthesis, the crystal structure refinement both from X-ray and neutron powder diffraction data and the electrical measurements of the $Pb_{1-x}Bi_xPt_2O_4$ series.

EXPERIMENTAL

Synthesis

A series of polycrystalline compounds with the compositions $Pb_{1-x}Bi_xPt_2O_4$ ($x = 0.0$, 0.1, 0.2, 0.3, 0.4, 0.5) were prepared by solid-state reaction. Stoichiometric quantities of PbO (Janssen 99.7%), Bi_2O_3 (Riedel 99.7%) and Pt metal (Aldrich 99.99%) according to

$$(1-x)\,PbO + \frac{x}{2}\,Bi_2O_3 + 2\,Pt + \left(\frac{3}{2} - \frac{x}{4}\right)O_2 \xrightarrow[1\ \text{week}]{680^\circ C} Pb_{1-x}Bi_xPt_2O_4$$

were thoroughly mixed in an agate mortar and heated in air, at 600°C for 24 h, then at 640°C for 48 h and finally at 680°C for 1 week with regrinding after each heating step. All samples were controlled at room temperature by X-ray powder diffraction using a Guinier-De Wolff focusing camera and Cu$K\alpha$ radiation. Unit-cell parameters were determined with a Siemens D5000 powder diffractometer (Cu$K\alpha$ radiation) equipped with a back monochromator and were least-squares refined after $K\alpha_2$ correction.

X-Ray Powder Diffraction

The crystal structure of the $x = 0.3$ term of the solid solution was refined from powder data recorded on a Siemens D5000 diffractometer using the same conditions of data collection and refinement than for $PbPt_2O_4$ investigation (3), and confirms the results obtained for $PbPt_2O_4$ compound.

Thermal Analysis

Differential thermal measurements were carried out in air on a SETARAM 92-1600 thermal analyzer in the temperature range 20–830°C both on heating and cooling.

Neutron Powder Diffraction

The neutron powder diffraction patterns of the compounds $x = 0$ and 0.3 were collected at room temperature using the high-resolution D2B powder diffractometer at *Institute Laue Langevin* (ILL), Grenoble. The high-intensity mode was used to collect the patterns at 298 K. The incident neutron wavelength, 1.594 Å, was selected from the (533) plane of a germanium single-crystal monochromator. About 5 g of each sample was enclosed in a vanadium cylindrical 8 mm diameter can. The 64 counters spaced at 2.5° intervals, were moved by step of 0.05° in the range $2.5^\circ \le 2\theta \le 162.5^\circ$. The counting times were 15 h for $PbPt_2O_4$ and 12 h for the substituted compound, respectively, and a total of 3240 data points were recorded. Both neutron diffraction patterns were refined by the Rietveld method (12, 13), using the Fullprof program (14), a strongly modified version of the Young and Wiles refinement program (15). A Gaussian function was chosen to generate the line shape of the diffraction peaks. The Gaussian component has widths given by the function $(FWHM)^2 = U\tan^2\theta + V\tan\theta + W$ (16), where U, V, and W are refineable parameters. The coherent scattering lengths used were 9.400, 8.526, 9.630 and 5.805 fm for Pb, Bi, Pt and O, respectively. The background was defined by fifth-order polynomial in 2θ and was refined simultaneously with the other profile parameters. The profile refinements were performed in the space group $P\bar{1}$, taking as starting model that of $PbPt_2O_4$ resulting from powder X-ray crystal structure determination (3). Cell dimensions and structural para-

TABLE 1
Crystal and Refinement Parameters from Neutron Diffraction Patterns for $PbPt_2O_4$ and $Pb_{0.7}Bi_{0.3}Pt_2O_4$

Chemical formula	$PbPt_2O_4$	$Pb_{0.7}Bi_{0.3}Pt_2O_4$
Formula weight (g mol^{-1})	661.36	661.90
Crystal system	Triclinic	Triclinic
Space group	*P*-1	*P*-1
Unit-cell dimensions		
a (Å)	6.1173(2)	6.1055(2)
b (Å)	6.6489(3)	6.6156(3)
c (Å)	5.5523(2)	5.5597(2)
α (deg)	97.195(3)	97.175(3)
β (deg)	108.827(3)	108.863(3)
γ (deg)	115.213(3)	115.214(3)
V (Å^3)	184.06(1)	182.99(2)
Unit formula	$Z = 2$	$Z = 2$
Density (g cm^{-3})	11.94 (2)	12.01(2)
Sample description	Black powder	Black powder
No. of fitted parameters	96	97
No of profile points	3240	3240
Half-width parameters		
U	0.086(7)	0.137(7)
V	0.053(9)	− 0.022(6)
W	0.062(4)	0.066(4)
R factors		
R_{exp}	0.017	0.029
R_p	0.039	0.057
R_{wp}	0.050	0.074
R_F	0.030	0.037
R_B	0.052	0.059

TABLE 2
Final Atomic Positions, Occupancy Factors, and Equivalent Isotropic Displacement Parameters Refined from Powder Neutron Diffraction for $PbPt_2O_4$ and $Pb_{0.7}Bi_{0.3}Pt_2O_4$

Atom	Site	x	y	z	B_{eq}(Å^2)[a]	Occup.
$PbPt_2O_4$						
Pb	2*i*	0.7471(7)	0.8594(7)	0.1365(7)	1.53(3)	1
Pt1	1*g*	0	$\frac{1}{2}$	$\frac{1}{2}$	1.30(2)	1
Pt2	1*f*	$\frac{1}{2}$	0	$\frac{1}{2}$	1.19(2)	1
Pt3	1*c*	0	$\frac{1}{2}$	0	1.54(2)	1
Pt4	1*h*	$\frac{1}{2}$	$\frac{1}{2}$	$\frac{1}{2}$	1.39(2)	1
O1	2*i*	0.605(1)	0.280(1)	0.364(1)	1.18(6)	1.01(1)
O2	2*i*	0.345(1)	0.503(1)	0.122(1)	1.80(5)	0.98(1)
O3	2*i*	0.159(1)	0.845(1)	0.167(1)	1.67(6)	0.99(1)
O4	2*i*	0.135(1)	0.273(1)	0.477(1)	1.12(5)	1.00(1)
$Pb_{0.7}Bi_{0.3}Pt_2O_4$						
Pb/Bi	2*i*	0.7449(7)	0.8592(7)	0.1320(8)	1.53(4)	0.71/0.29(1)
Pt1	1*g*	0	$\frac{1}{2}$	$\frac{1}{2}$	1.62(3)	1
Pt2	1*f*	$\frac{1}{2}$	0	$\frac{1}{2}$	0.89(2)	1
Pt3	1*c*	0	$\frac{1}{2}$	0	1.55(2)	1
Pt4	1*h*	$\frac{1}{2}$	$\frac{1}{2}$	$\frac{1}{2}$	1.17(2)	1
O1	2*i*	0.604(1)	0.276(1)	0.363(1)	1.81(5)	1.01(2)
O2	2*i*	0.346(1)	0.507(1)	0.127(1)	1.76(6)	0.98(1)
O3	2*i*	0.164(1)	0.848(1)	0.171(1)	1.49(4)	0.97(1)
O4	2*i*	0.136(1)	0.273(1)	0.477(1)	1.09(5)	0.97(2)

[a] $B_{eq} = \frac{4}{3} \sum_i \sum_j \beta_{ij} a_i a_j$.

meters were refined, with independent refinement of the profile parameters, i.e. peak shapes, background parameters, zero-point correction and scale factors. In the final refinement, anisotropic thermal parameters were refined for all atoms. Crystal and refinement parameters are summarized in Table 1. The final refined atomic positions, occupancy factors and equivalent isotropic displacement parameters are shown in Table 2, anisotropic displacement parameters for all atoms in Table 3, with selected bond lengths and angles in Table 4. The corresponding fitted diffraction diagrams are shown in Fig. 1. We notice a weak increase of the background with 2θ values, it is probably due to the elastic diffuse scattering contributions.

Electrical Measurements

The electrical conductivity of four samples ($x = 0$, 0.1, 0.2 and 0.3) was measured on sintered pellets using a standard four-point technique in the range 4.2–300 K. Contact of the four leads was achieved through a silver paint. The sample was supplied by a current source with a current of 1 mA, which corresponds to a current density of about 0.02 A cm^{-2} and the voltage was measured with a nanovoltmeter.

Lone-Pair Electrons Localization

The phenomenon of the lone-pair electrons occurs in solid-state materials containing heavy metal cations of the *p* block with an external electronic configuration ns^2np^0 such as Bi^{3+} and Pb^{2+}. This pair occupies approximately the same volume that an anion O^{2-} or F^-. As its electronic

TABLE 3
Anisotropic Displacement Parameters β_{ij}[a] Refined from Powder Neutron Diffraction for $PbPt_2O_4$ and $Pb_{0.7}Bi_{0.3}Pt_2O_4$

Atom	β_{11}	β_{22}	β_{33}	β_{12}	β_{13}	β_{23}
$PbPt_2O_4$						
Pb	0.0135(14)	0.0136(15)	0.0087(16)	0.0067(12)	0.0046(14)	0.0014(12)
Pt1	0.0042(23)	0.0200(20)	0.0029(20)	0.0037(09)	− 0.0009(09)	0.0055(09)
Pt2	0.0076(19)	0.0074(16)	0.0140(22)	0.0030(08)	0.0027(09)	− 0.0023(09)
Pt3	0.0039(22)	0.0154(22)	0.0134(23)	0.0028(09)	− 0.0004(08)	− 0.0004(09)
Pt4	0.0040(18)	0.0195(22)	0.0063(19)	0.0023(09)	0.0019(17)	0.0042(09)
O1	0.0089(26)	0.0158(24)	0.0150(29)	0.0086(20)	0.0088(21)	0.0124(20)
O2	0.0221(27)	0.0090(19)	0.0066(28)	0.0002(17)	0.0038(22)	− 0.0027(19)
O3	0.0271(32)	0.0081(18)	0.0042(24)	0.0012(19)	0.0094(20)	− 0.0009(19)
O4	0.0115(25)	0.0065(23)	0.0005(21)	− 0.0019(18)	− 0.0016(19)	− 0.0013(16)
$Pb_{0.7}Bi_{0.3}Pt_2O_4$						
Pb, Bi	0.0119(15)	0.0141(15)	0.0117(17)	0.0050(12)	0.0047(14)	0.0007(12)
Pt1	0.0061(27)	0.0203(21)	0.0022(21)	0.0067(20)	0.0029(19)	0.0056(17)
Pt2	0.0021(18)	0.0052(15)	0.0108(21)	0.0005(15)	0.0001(16)	− 0.0037(15)
Pt3	0.0043(22)	0.0122(22)	0.0170(25)	0.0050(17)	0.0006(16)	− 0.0007(18)
Pt4	0.0030(02)	0.0166(21)	0.0044(19)	0.0011(17)	0.0015(16)	0.0035(17)
O1	0.0138(22)	0.0222(25)	0.0125(28)	0.0101(19)	0.0033(19)	0.0114(21)
O2	0.0117(25)	0.0060(08)	0.0239(34)	− 0.0017(17)	0.0068(23)	0.0030(23)
O3	0.0217(32)	0.0041(21)	0.0024(26)	0.0001(19)	0.0007(21)	− 0.0072(18)
O4	0.0091(25)	0.0075(24)	0.0051(25)	− 0.0004(19)	0.0022(21)	− 0.0037(18)

[a] The anisotropic displacement exponent takes the form $(\beta_{11}h^2 + \beta_{22}k^2 + \beta_{33}l^2 + \beta_{12}hk + \beta_{13}hl + \beta_{23}kl)$.

TABLE 4
Selected Bond Lengths (Å) and Angles (°) for $PbPt_2O_4$ and $Pb_{0.7}Bi_{0.3}Pt_2O_4$

	$PbPt_2O_4$	$Pb_{0.7}Bi_{0.3}Pt_2O_4$		$PbPt_2O_4$	$Pb_{0.7}Bi_{0.3}Pt_2O_4$
Pb–Bi environment			$O(1)^0$–Pt(2)–$O(3)^{i}$	86.1(4)	85.4(5)
Pb–$O(1)^{ix}$	2.649(7)	2.625(7)	$O(1)^0$–Pt(2)–$O(3)^{iii}$	93.9(4)	94.6(5)
Pb–$O(2)^0$	2.553(8)	2.543(8)	Pt3 environment		
Pb–$O(2)^{ix}$	2.377(8)	2.394(8)	Pt(3)–$O(2)^{0,iv} \times 2$	1.989(8)	1.976(8)
Pb–$O(3)^{x}$	2.516(9)	2.534(9)	Pt(3)–$O(3)^{0,iv} \times 2$	2.011(7)	2.022(7)
Pb–$O(3)^{viii}$	2.744(7)	2.718(8)	⟨Pt(3)–O⟩	2.000(7)	1.999(7)
Pb–$O(4)^{vii}$	2.645(7)	2.652(7)	$O(2)^0$–Pt(3)–$O(3)^{iv}$	95.4(5)	93.9(5)
Pb–$O(4)^{i}$	2.432(7)	2.452(7)	$O(2)^0$–Pt(3)–$O(3)^0$	84.6(5)	86.1(5)
⟨Pb–O⟩	2.559(8)	2.560(8)	Pt4 environment		
$O(1)^{ix}$–Pb–$O(2)^0$	77.4(3)	78.7(4)	Pt(4)–$O(1)^{0,i} \times 2$	1.987(6)	2.004(7)
$O(1)^{ix}$–Pb–$O(2)^{ix}$	66.5(3)	67.3(4)	Pt(4)–$O(2)^{0,i} \times 2$	2.010(6)	1.994(7)
$O(1)^{ix}$–Pb–$O(3)^{x}$	112.4(5)	113.6(5)	Pt(4)–$O(4)^{0,i} \times 2$	2.047(6)	2.033(7)
$O(1)^{ix}$–Pb–$O(3)^{viii}$	61.4(3)	60.6(3)	⟨Pt(4)–O⟩	2.015(6)	2.010(7)
$O(1)^{ix}$–Pb–$O(4)^{vii}$	133.6(4)	133.9(4)	$O(1)^0$–Pt(4)–$O(2)^0$	87.6(5)	88.4(5)
$O(1)^{ix}$–Pb–$O(4)^{i}$	143.0(4)	143.6(4)	$O(1)^0$–Pt(4)–$O(2)^{i}$	92.4(4)	91.6(5)
$O(2)^0$–Pb–$O(2)^{ix}$	65.5(4)	66.8(4)	$O(1)^0$–Pt(4)–$O(4)^0$	101.3(5)	100.9(5)
$O(2)^0$–Pb–$O(3)^{x}$	120.8(5)	121.4(5)	$O(1)^0$–Pt(4)–$O(4)^{i}$	78.7(4)	79.0(4)
$O(2)^0$–Pb–$O(3)^{viii}$	136.7(5)	137.1(5)	$O(2)^0$–Pt(4)–$O(4)^0$	92.6(4)	92.7(5)
$O(2)^{ix}$–Pb–$O(3)^{x}$	66.7(4)	67.2(4)	$O(2)^0$–Pt(4)–$O(4)^{i}$	87.4(4)	87.3(5)
$O(2)^{ix}$–Pb–$O(3)^{viii}$	105.9(4)	105.6(4)			
$O(2)^0$–Pb–$O(4)^{vii}$	138.6(4)	137.0(4)	O environment		
$O(2)^0$–Pb–$O(4)^{i}$	68.4(3)	67.6(4)	O(1)–$O(2)^0$	2.767(9)	2.787(9)
$O(2)^{ix}$–Pb–$O(4)^{vii}$	143.9(4)	143.2(5)	O(1)–$O(2)^{i}$	2.885(9)	2.867(9)
$O(2)^{ix}$–Pb–$O(4)^{i}$	86.3(4)	86.5(4)	O(1)–$O(3)^{iii}$	2.753(9)	2.696(9)
$O(3)^{x}$–Pb–$O(3)^{viii}$	88.7(4)	89.1(4)	O(1)–$O(3)^0$	2.948(8)	2.921(2)
$O(3)^{x}$–Pb–$O(4)^{vii}$	77.3(4)	76.1(4)	O(1)–$O(4)^{i}$	2.559(8)	2.570(8)
$O(3)^{x}$–Pb–$O(4)^{i}$	75.7(4)	75.4(4)	O(2)–$O(2)^{ix}$	2.672(9)	2.720(9)
$O(3)^{viii}$–Pb–$O(4)^{vii}$	74.2(3)	75.2(3)	O(2)–$O(3)^{iv}$	2.692(9)	2.729(9)
$O(3)^{viii}$–Pb–$O(4)^{i}$	154.8(4)	155.1(4)	O(2)–$O(3)^0$	2.959(9)	2.923(9)
$O(4)^{i}$–Pb–$O(4)^{vii}$	83.0(3)	82.1(3)	O(2)–$O(4)^{i}$	2.803(9)	2.780(2)
Pt1 environment			O(2)–$O(4)^0$	2.933(9)	2.915(9)
Pt(1)–$Pt(3)^{0,xii} \times 2$	2.776(1)	2.780(1)	Pt(1)^{x}–O(1)–$Pt(2)^0$	115.8(3)	116.3(3)
Pt(1)–$O(1)^{i,v} \times 2$	2.020(7)	2.022(7)	Pt(1)^{x}–O(1)–$Pt(4)^0$	99.5(3)	98.6(3)
Pt(1)–$O(4)^{0,vi} \times 2$	2.014(6)	2.012(7)	$Pt(2)^0$–O(1)–$Pt(4)^0$	111.9(3)	111.5(3)
⟨Pt(1)–O⟩	2.017(7)	2.017(7)	$Pt(3)^0$–O(2)–$Pt(4)^0$	116.6(3)	117.8(3)
$O(1)^{v}$–Pt(1)–$O(4)^0$	101.2(5)	100.9(5)	Pt(2)^{xi}–O(3)–$Pt(3)^0$	116.3(5)	116.7(3)
$O(1)^{i}$–Pt(1)–$O(4)^0$	78.8(4)	79.1(4)	$Pt(1)^0$–O(4)–$Pt(4)^0$	97.7(3)	98.0(3)
Pt2 environment					
Pt(2)–$O(1)^{0,ii} \times 2$	2.025(6)	1.997(6)			
Pt(2)–$O(3)^{i,iii} \times 2$	2.008(6)	1.978(6)			
⟨Pt(2)–O⟩	2.052(6)	1.987(6)			

Note. For symmetry codes see Table 5.

density is weak, the diffraction does not allow to localize it. A method of location based on the balance of the electrostatic interactions in the material, has been proposed by Verbaere *et al.* (17). Assuming that the polarizability of a ns^2np^0 atom results essentially from the presence of the lone-pair electrons, the electric dipolar moment can be assimilated to the polarization induced by the local crystal field to which it is submitted ($P = -2d = \alpha E$), where -2 is the charge of lone pair, d the distance to the nucleus of the atom supporting the pair, α the electronic polarizability of the ion proposed by Shannon (18) and E is the local electric field in the crystal. This method worked well for a simple oxides such as PbO and for double oxides (19, 20)

The lone-pair electrons localization was carried out with the program HYBRIDE (21) based on the algorithm of Verbaere *et al.* (17), in which E is calculated by the Ewald method (22), where the polarizability of Pb^{2+} and Bi^{3+} chosen are 6.58 and 6.12 $Å^3$, respectively. The calculation used to determine ions partial charges derives from the Pauling empirical formula (23), that gives the ionicity rate of a bond M–O according to the difference between the electronegativity χ_M and χ_O of M and O atoms. Values of χ are

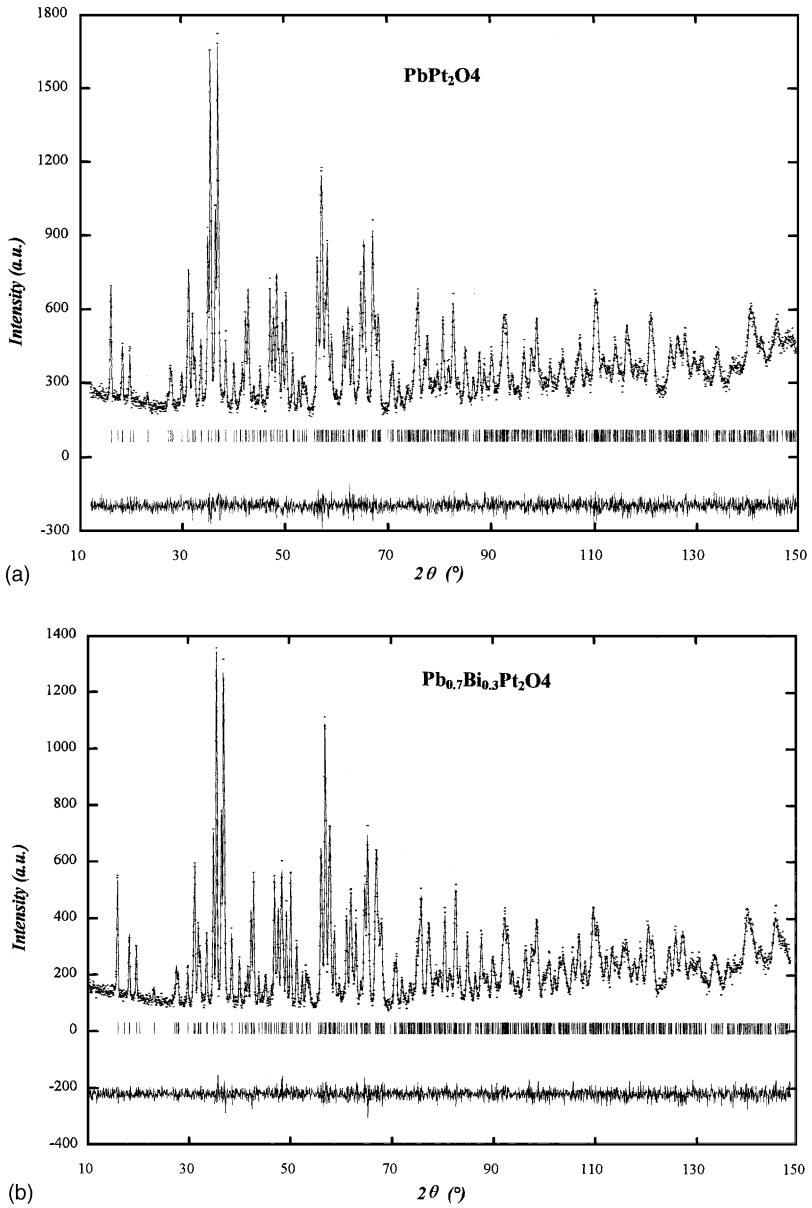

FIG. 1. Observed (points) and calculated (continuous line) neutron diffraction patterns of $PbPt_2O_4$ (a) and $Pb_{1-x}Bi_xPt_2O_4$ (b). The reflection markers and the difference patterns appear in the lower part.

taken in the electronegativity scale of Allred *et al.* (24). Thus, a per cent formal ionicity value was calculated for each bond using formula

$$M\text{–O} = 1 - \exp[-(\chi_O - \chi_M)^{2/4}].$$

From atomic positions obtained by neutron diffraction, the location of the lone pairs of the Pb/Bi atoms was determined using the calculation method described above and the oxygen environments of Pb/Bi are discussed. For the substituted compound, the calculation was undertaken allocating the polarized atom of an average polarizability coefficient value and an average charge, that takes into account the substitution rate in this site. This charge was compensated supposing a reduction of platinum atoms along the Pt(1)–Pt(3) chain to respect the electrical neutrality of the material. The refinement of the lone-pair position and its environment is given in Table 5.

RESULTS AND DISCUSSION

The phase analysis of the different samples by X-ray diffraction showed the existence of a solid solution and the quaternary oxides ($Pb_{1-x}Bi_xPt_2O_4$) were obtained as single

TABLE 5
Lone Pair (Lp) Position, Distances Lp–O < 3 Å, and Angles Lp–Pb–O

	Lp position	Lp–O	Distances (Å)	Lp–Pb–O angles (deg)
$PbPt_2O_4$		Lp–Pb	0.98(1)	
		Lp–O(1)^{xi}	2.56(1)	17.9(7)
		Lp–O(1)^{xix}	2.84(1)	91.4(7)
	$x = 0.660(4)$	Lp–O(2)^{0}	2.56(1))	79.5(8)
	$y = 0.935(5)$	Lp–O(3)^{viii}	2.80(1)	29.0(8)
	$z = 0.200(4)$	Lp–O(3)^{0}	2.89(1))	88.3(8)
		Lp–O(4)^{vii}	2.56(1)	74.0(7)
		Lp–O(4)^{i}	2.71(1))	95.7(8))
$Pb_{0.7}Bi_{0.3}Pt_2O_4$		Lp–(Pb,Bi)	0.89(1)	
		Lp–O(1)^{xi}	2.59(1)	16.4(7)
		Lp–O(1)^{xix}	2.78(1)	90.8(7)
	$x = 0.667(5)$	Lp–O(2)^{0}	2.54(1)	79.9(8)
	$y = 0.931(4)$	Lp–O(3)^{viii}	2.85(1)	29.4(7)
	$z = 0.188(4)$	Lp–O(3)^{0}	2.82(1)	87.2(8)
		Lp–O(4)^{vii}	2.55(1)	73.4(8)
		Lp–O(4)^{i}	2.69(1)	96.2(8)

Note. Symmetry codes: (0) x, y, z, (i) $1-x, 1-y, 1-z$; (ii) $1-x, -y, 1-z$; (iii) $x, -1+y, z$; (iv) $-x, 1-y, -z$; (v) $-1+x, y, z$; (vi) $-x, 1-y, 1-z$; (vii) $1+x, 1+y, z$; (viii) $1-x, 2-y, -z$; (ix) $1-x, 1-y, -z$; (x) $1+x, y, z$; (xi) $x, 1+y, z$.

phases for $x \leq 0.3$, while for $x > 0.3$, a second phase, $Pb_{2-x}Bi_xPtO_4$, was observed on the X-ray diffraction diagram. To follow the evolution of the cell parameters, several compounds for various compositions ($x = 0.00$, 0.10, 0.15, 0.20, 0.25 and 0.30) were synthetized. The refinement of the cell parameters, using a least-squares procedure, shows a weak evolution of these parameters: a, b and the volume V decrease in a linear way with the substitution rate while c increases. The evolution of these parameters is given in Fig. 2.

The differential thermal analysis study of two compounds ($x = 0$ and 0.3), Figs. 3a and 3b, showed that when the samples are heated, an endothermic peak due to decomposition of compounds is observed at 784°C for $PbPt_2O_4$ and 780°C for $Pb_{0.7}Bi_{0.3}Pt_2O_4$. The analysis of residues by X-ray diffraction after DTA, shows the existence of PbO and platinum for $x = 0$ plus bismuth oxide Bi_2O_3 for $x = 0.3$.

The refinement of the crystal structure of $Pb_{0.7}Bi_{0.3}Pt_2O_4$ from the powder X-ray diffraction pattern using the Rietveld method confirms the essential features of the structure of $PbPt_2O_4$. The crystal structure is constituted by four independent platinum atoms in special positions, one mixed lead-bismuth site and four oxygen sites, in general positions. In this structure, the platinum atoms (Fig. 4) present two different environments, square planes for Pt(1)–Pt(3) atoms while Pt(4) is in an octahedral environment. The $Pt(1)O_4$ and $Pt(3)O_4$ units are alternatively stacked along [001], and they are twisted to each other by 45°. The resulting columns of PtO_4 units are connected by $Pt(2)O_4$ units to form a Pt_3O_8 layer parallel to the $(1\bar{1}0)$ plane (Fig. 4). A $Pt(2)O_4$ square shares two oxygen atoms with one $Pt(1)O_4$ and one $Pt(3)O_4$ unit of one column and the two others with two successive PtO_4 units of the nearby column. The layers are connected by $Pt(4)O_6$ octahedrons to form a tri-dimensional network. The Pb/Bi atoms occupy the large elliptic tunnels created by this network. The Pb^{2+}/Bi^{3+} ions fit very well in the oxygen channels, as shown by the Pb/Bi–O bond lengths.

Contrary to the diffraction of X rays, the diffraction of neutrons allows to differentiate the lead atoms and the bismuth atoms. The refinement of the rate of occupation of the Pb/Bi site in the case of $x = 0.3$ confirms the formula and the existence of the solid solution. On the other hand, the refinement using neutron diffraction data of the occupa-

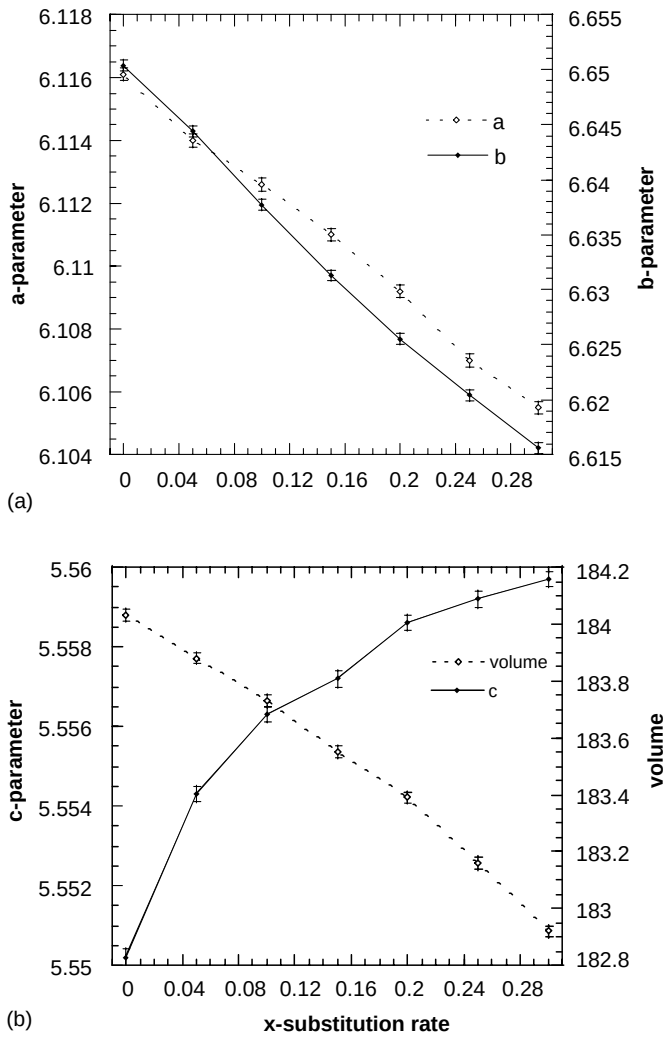

FIG. 2. Volume and cell parameters evolution for the $Pb_{1-x}Bi_xPt_2O_4$ series ($0 \leq x \leq 0.3$): (a) cell parameters a and b; (b) volume v and cell parameter c.

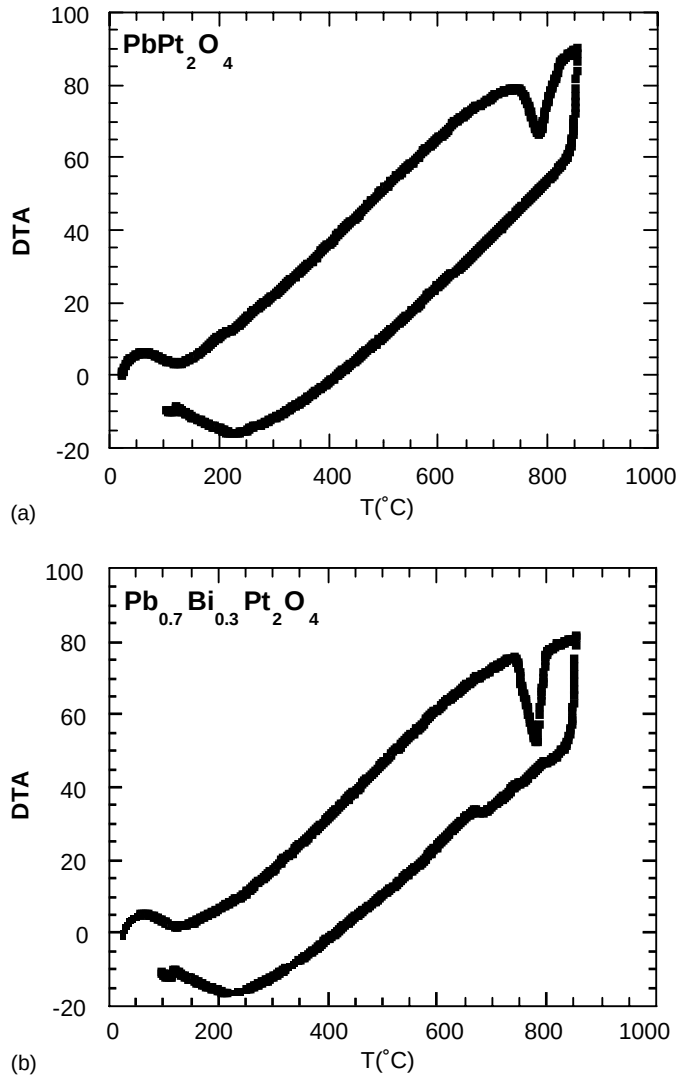

FIG. 3. Differential thermal analysis study for $PbPt_2O_4$ (a) and $Pb_{0.7}Bi_{0.3}Pt_2O_4$ (b).

tion rates of oxygen sites does not allow to detect any non-stoichiometry in oxygen in the pure phase but also in the substituted compound. So, in the series $Pb_{1-x}Bi_xPt_2O_4$ the excess of charge introduced by the substitution of Pb^{2+} for Bi^{3+} is compensated by a possible reduction of platinum atoms. A charge-distribution model for the platinum atoms can be proposed with Pt^{4+} in octahedral site, Pt^{2+} in isolated square plane and an unique non-integer formal oxidation state for Pt(1) and Pt(3) which ranges from $+3$ for $PbPt_2O_4$ to $+2.7$ for the $Pb_{0.7}Bi_{0.3}Pt_2O_4$ limit composition. This hypothesis allows to explain the opposite evolutions of the unit-cell parameters, the decrease of a and b translates the decrease of the ionic radii of bismuth compared to lead while the weak increase of c is due to the reduction of the platinum, such an evolution of the distance platinum–platinum ($c/2$) according to the average oxidation degree of the platinum has already been observed, for example, in the series $Bi_{2-x}Pb_xPtO_4$ (6). The non-integer oxidation state of platinum along the Pt(1)–Pt(3) chain is allowed by the delocalization of outer d electrons in the columnar stacked PtO_4 substructure with a strong cation–cation interaction resulting from the small Pt–Pt separation of 2.78 Å (the distance Pt–Pt found in platinum metal is 2.775 Å). Partial oxidation of the platinum in the Pt(1)/Pt(3) linear chains results in the removal of electrons from the top of the d_{z^2} band promoting metallic conductivity. In fact, all well characterized platinum oxides containing square-planar stacking columns extending along two or three

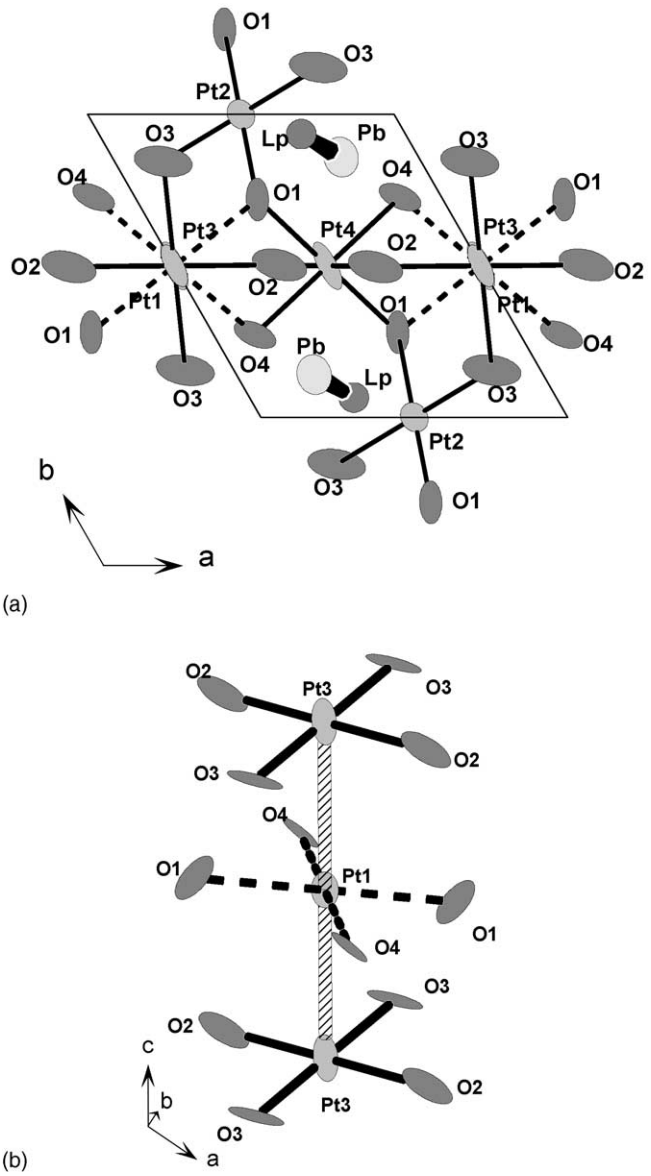

FIG. 4. (a) Projection of the $PbPt_2O_4$ crystal structure along the [001] direction showing the network built from PtO_4 and PtO_6 entities. (b) Pt(1) and Pt(3) environments along the c-axis.

crystallographic directions are metallic, such as the platinum bronzes $Na_xPt_3O_4$ (25) or $CaPt_2O_4$ (26). For one-dimensional metallic interactions, the partially filled band splits into one totally filled band and one empty with a gap between the two bands (Peierls theorem), so the compounds with columnar stacks of Pt–Pt chains in only one direction exhibit a semiconducting behavior with, however high-conductivity values ($\sigma \approx 10$–$100\ \Omega^{-1}\ cm^{-1}$). The decrease of the Pt(2)–O average distance from 2.016 to 1.988 Å upon addition of Bi is the greatest change between the two structures. This may reflect an altered lone-pair–Pt(2) interaction confirmed by the increase of the Lp–Pt(2) distance from 2.27 to 2.37 Å for $PbPt_2O_4$ and $Pb_{0.7}Bi_{0.3}Pt_2O_4$, respectively.

The temperature dependence of the specific resistivity (ρ) for sintered pellets of $Pb_{1-x}Bi_xPt_2O_4$ solid solution is shown in Fig. 5. Since no significant hysterisis was observed between the cooling and heating process, only the heating curves are represented. Several interesting observations can be made from the electrical data. The three first compounds ($x = 0$, 0.1 and 0.2) exhibit a metallic behavior, the electrical resistivity increases with increasing temperature. Their room temperature resistivities are, respectively, 1.5×10^{-2}, 2.1×10^{-2} and $2.9 \times 10^{-2}\ \Omega$ cm. At a given temperature, we observe an increasing of the resistivity with the bismuth substitution rate. The electrical behavior drastically changes for the maximum substituted compound, $x = 0.3$. A very large increase of resistivity is observed (28.2 Ω cm at room temperature) with an electrical vs temperature behavior change, the resistivity decreases with increasing temperature. The negative temperature dependence and the relatively high-resistivity values suggests that this compound is a semiconductor. Thus, a transition from metallic to semiconductivity properties is observed for x close to 0.3.

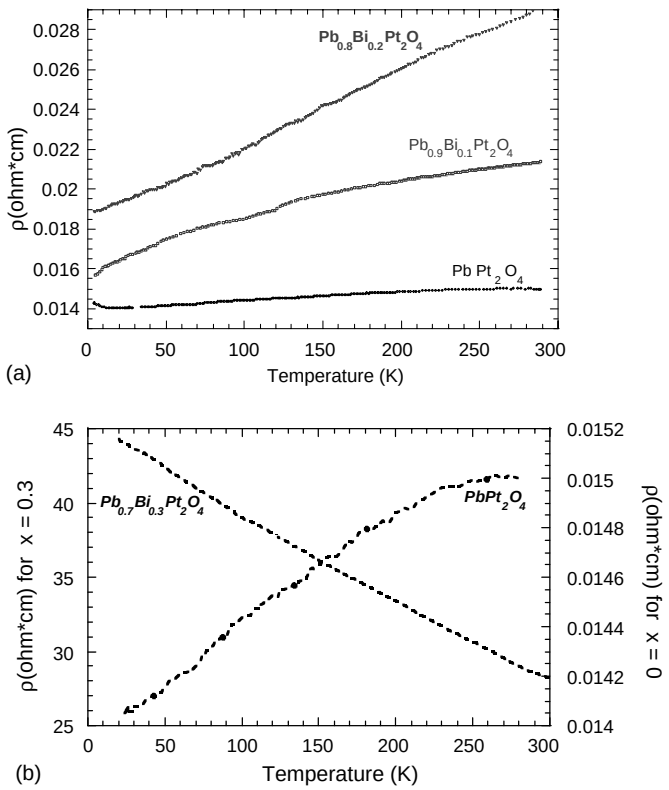

FIG. 5. Temperature dependence of the resistivity for the $Pb_{1-x}Bi_xPt_2O_4$ series: (a) $x = 0$, 0.1 and 0.2, (b) $x = 0.3$ and 0 with a large scale.

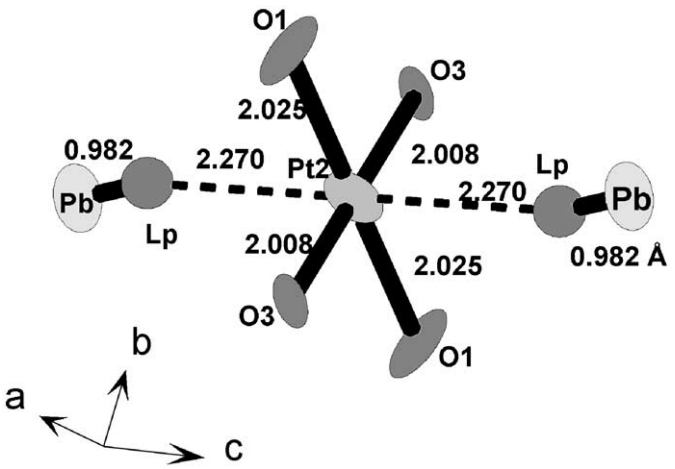

FIG. 6. The distorted octahedral Pt(2) atom environment involving the electronic lone pair of the Pb^{2+} ion in $PbPt_2O_4$.

The mixed site Pb/Bi is surrounded by seven oxygen atoms to form a very distorted polyhedron. The polyhedron is completed by the lone-pair Lp which occupies the free space around Bi/Pb. The lone pairs are directed towards the Pt(2) atom and completes the coordination around Pt(2) to form an elongated octahedron $Pt(2)O_4Lp_2$ (Fig. 6). Two $(Pb–Bi)O_7Lp$ polyhedrons are connected by an O(4)–O(4) edge to form a dimer $(Pb–Bi)_2O_{12}$ (Fig. 7).

CONCLUSION

An extensive new solid solution was prepared in which Pb^{2+} is replaced by Bi^{3+} in the $PbPt_2O_4$ compound. Refinement of the crystal structure of the two limits of the solid solution from neutron diffraction data did not allow to discover any non-stoichiometry in oxygen and seems to confirm the formula $Pb_{1-x}Bi_xPt_2O_4$. So the replacement of Bi for Pb comes along with a partial reduction of the atoms of platinum constituting the planar stack of PtO_4 groups extending along the [001] direction. The electric properties evolve from a metal behavior for $x = 0$ towards a semiconducting behavior for $x = 0.3$. The growth of single crystals would allow to verify the mono-dimensional character of the specific conductivity.

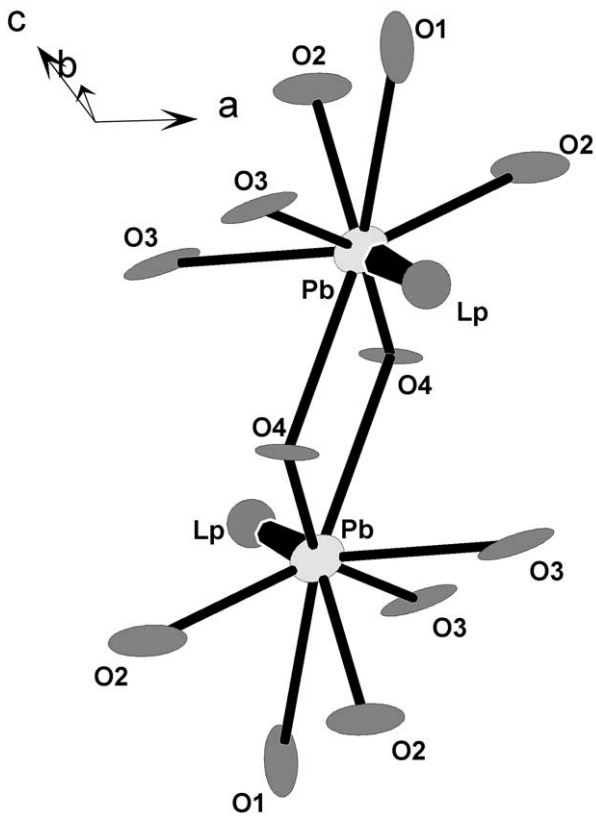

FIG. 7. Two (Pb–Bi)O_7Lp polyhedrons share an O(4)–O(4) edge to form a (Pb–Bi)$_2O_{12}Lp_2$ dimeric unit.

REFERENCES

1. K. B. Schwartz and C. T. Prewitt, *J. Phys. Chem. Solid* **45**(1), 1 (1984).
2. N. Bettahar, P. Conflant, F. Abraham, and D. Thomas, *J. Solid State Chem.* **67,** 85 (1987).
3. N. Tancret, S. Obbade, N. Bettahar, and F. Abraham, *J. Solid State Chem.* **124,** 309 (1996).
4. A. W. Sleight, *Mater. Res. Bull.* **9,** 1177 (1974).
5. F. Abraham, D. Thomas, and G. Nowogrocki, *Bull. Soc. Fr. Miner. Crystallogr.* **98,** 25 (1975).
6. N. Bettahar, P. Conflant, J. C. Boivin, F. Abraham, and D. Thomas, *Chem. Phys. Solids* **46,** 297 (1985).
7. J. C. Boivin, P. Conflant, and D. Thomas, *Mater. Res. Bull.* **11,** 1503 (1976).
8. P. Conflant, J. C. Boivin, and D. Thomas, *Rev. Chim. Miner.* **14,** 249 (1977).
9. J. C. Boivin, J. Tréhoux, and D. Thomas, *Bull. Soc. Fr. Miner. Crystallogr.* **99,** 193 (1976).
10. N. Bettahar, P. Conflant, and F. Abraham, *J. Alloys Compd.* **188,** 211 (1992).
11. N. Bettahar, Z. Derriche, F. Abraham, and P. Conflant, *Ann. Chim. Sci. Mater.* **25,** 297 (2000).
12. H. M. Rietveld, *Acta Crystallogr.* **22,** 151 (1967).
13. H. M. Rietveld, *Acta Crystallogr.* **25,** 589 (1992).
14. J. Rodrigez Carvajal, M. T. Fernandez Diaz, and J. L. Martinez, *J. Phys.: Condens. Matter* **3,** 3215 (1991).
15. D. B. Wiles and R. A. Young, *J. Appl. Crystallogr.* **14,** 149 (1981)/**15,** 430 (1982).
16. C. Caglioti, A. Paoletti, and E. P. Ricci, *Nucl. Instrum. Methods* **3,** 223 (1958).
17. A. Verbaere, R. Marchand, and M. J. Tournoux, *J. Solid State Chem.* **23,** 383 (1978).
18. R. D. Shannon, *J. Appl. Phys.* **73**(1), 348 (1993).
19. O. Mentré, A. C. Dahaussy, and F. Abraham, *Chem. Mater.* **11**(9), 2408 (1999).
20. S. Giraud, J. P. Wignacourt, S. Swinnea, H. Steinfink, and R. Harlow, *J. Solid State Chem.* **151,** 181 (2000).
21. E. Morin, G. Wallez, S. Jaulmes, J. C. Couturier, and M. Quarton, *J. Solid State Chem.* **137,** 283 (1998).
22. P. P. Ewald, *Ann. Phys.* **64,** 253 (1921).
23. L. Pauling, "The Nature of the chemical Bond," Cornell University Press, New York, 1939.
24. A. L. Allred and E. G. Rochow, *J. Inorg. Nucl. Chem.* **5,** 264 (1958).
25. K. B. Schwartz, C. T. Prewitt, R. D. Schannon, L. M. Corliss, J. M. Hastings, and B. Chamberland, *Acta Crystallogr. B* **38,** 363 (1982).
26. D. Cahen, J. A. Ibers, and M. H. Mueller, *Inorg. Chem.* **13,** 110 (1974).